

**Role of the entrance channel in the experimental study of incomplete fusion of  $^{13}\text{C}$  with  $^{93}\text{Nb}$** 

Avinash Agarwal<sup>1</sup>,\* Anuj Kumar Jashwal,<sup>†</sup> Munish Kumar, and S. Prajapati  
*Department of Physics, Bareilly College, Bareilly (U.P.) 243 005, India*

Sunil Dutt, Muntazir Gull, and I. A. Rizvi  
*Department of Physics, Aligarh Muslim University, Aligarh (U.P.) 202 002, India*


Kamal Kumar  
*Department of Physics, Hindu College, Moradabad (U.P.) 244 001, India*

Sabir Ali<sup>2</sup>  
*MANUU Polytechnic Darbhanga, Maulana Azad National Urdu University, Hyderabad 500 032, India*

Abhishek Yadav<sup>3</sup>  
*Department of Physics, Jamia Millia Islamia, New Delhi 110 025, India*

R. Kumar  
*NP-Group, Inter University Accelerator Center, New Delhi 110 067, India*

A. K. Chaubey<sup>4</sup>  
*Department of Physics, Addis Ababa University, P.O. Box 1176, Addis Ababa, Ethiopia*

 (Received 9 June 2021; revised 16 January 2022; accepted 25 February 2022; published 10 March 2022)

We report measured cross-section data of the residues produced in the  $^{13}\text{C}$ -induced reaction on  $^{93}\text{Nb}$  within the 63.7–87.1-MeV energy range. The off-line  $\gamma$ -ray spectroscopy method has been used to measure the cross sections of the radionuclides produced in this system. The analysis of present measured cross-section data has been carried out within the light of well-established statistical model code PACE4. The excitation function of residues populated via  $xn$  and/or  $pxn$  channels are found to be in fair agreement with those estimated by the theoretical model code, which confirms the assembly of these residues via complete fusion process. A considerable enhancement in the measured cross-section data has been observed for the residues involving  $\alpha$ -emitting channels as compared to the theoretical predictions. The observed enhancement in the cross sections has been assigned to the incomplete fusion processes. Furthermore, in order to have a better insight into the onset and strength of incomplete fusion, termed as the incomplete fusion fraction has been deduced for the present paper and is compared with  $^{16}\text{O}$  and  $^{18}\text{O}$  beams on the same target  $^{93}\text{Nb}$ . This suggests that the incomplete fusion fraction is strongly influenced by the entrance channel, which may be understood in terms of the projectile  $Q_\alpha$  value. The comparison of this paper with literature data also shows that the incomplete fusion probability increases with various entrance channel parameters, such as projectile structure, projectile energy, and mass asymmetry of interacting partners.

DOI: [10.1103/PhysRevC.105.034609](https://doi.org/10.1103/PhysRevC.105.034609)

**I. INTRODUCTION**

In recent years, appreciable efforts have been dedicated to understand the fusion dynamics in heavy-ion (HI) interactions at energies above the Coulomb barrier [1,2]. It is now experimentally verified that complete fusion (CF) and incomplete fusion (ICF) are the foremost dominating modes in HI interaction at energies above the Coulomb barrier [3,4].

However, recent studies [5–10] show that ICF reactions contribute significantly in the production cross-section values of experimentally measured total cross-section ( $\sigma_T$ ) data. In contrast to complete fusion process where an entire amalgamation of the projectile or all its fragments with the target nucleus takes place, and in the ICF process the entire transfer of mass, linear, or angular momentum does not occur. Therefore, a combined and consistent description of CF and ICF is important to get acquainted about the transfer of energy, mass, linear, and angular momentum in nuclear reactions. It is an experimental challenge to unambiguously separate the ICF component from the CF events in a nuclear reaction.

\*Corresponding author: avibcb@gmail.com

<sup>†</sup>Corresponding author: anuj3674@gmail.com

The primary evidence of ICF was given by Britt and Quinton [11], when performing the experiment with  $^{12}\text{C}$ ,  $^{14}\text{N}$ , and  $^{16}\text{O}$  projectile beams at energy  $\approx 7\text{--}10$  MeV/A. A variety of dynamical models have been developed to describe the ICF dynamics in HI collisions, just like the breakup fusion model [12], the sum-rule model [13], the promptly emitted particles model [14], the exciton model [15], the hot spot model [16]. The CF and ICF processes also can be understood on the idea of driving input angular momenta imparted into the system. The CF occurs for the input angular momenta values  $\leq \ell_{\text{crit}}$ , as per the sharp cutoff approximation. However, at relatively higher projectile energies and/or at larger impact parameters, the ICF process starts competing with CF. It may, further, be acknowledged that the multitude of driving input angular momenta may vary with the projectile energy and/or with the impact parameter. However, there is no sharp boundary for the CF and ICF processes as both processes have been observed below and/or above the limiting value of input angular momenta [17]. Parker *et al.* [18] observed forward  $\alpha$  particles in the interaction of  $^{12}\text{C}$ ,  $^{15}\text{N}$ ,  $^{16}\text{O}$ ,  $^{19}\text{F}$ , and  $^{20}\text{Ne}$  with a  $^{51}\text{V}$  target at energies of 6 MeV/A. Some other studies [19–23] have also reported the existence of ICF at energies just above the Coulomb barrier and dependency of ICF strength fraction  $F_{\text{ICF}}$  on different entrance channel parameters. It is pointed out that besides several radioisotopes, the cross section for the production of  $^{97}\text{Ru}$  has also been measured. The  $^{97}\text{Ru}$  radioisotope is found to be the most suited radioisotope for medical purpose. The combination of excellent physical and chemical properties of  $^{97}\text{Ru}$  made it appealing for labeling compounds for delayed studies in diagnostic as well as therapeutic applications [24,25]. Morgenstern *et al.* [26] concluded that a more mass-asymmetric system has relatively higher ICF contribution than that of a less mass-asymmetric system at the constant relative velocity. The effect of projectile structure on the ICF process has been investigated by Singh *et al.* [27]. Furthermore, the importance of projectile structure on ICF is explored more effectively in terms of projectile  $Q_\alpha$  value [20,22,23]. The study carried out by Shuaib *et al.* [28] suggest that ICF probability increases with an increasing in the product of the projectile and target charge  $Z_p Z_T$  (Coulomb factor).

In the present paper, for better insight into the ICF dependence on various entrance channel parameters, we have measured the excitation functions (EFs) of various evaporation residues (ERs) populated in the interaction of the  $^{13}\text{C} + ^{93}\text{Nb}$  system. The measured EFs are analyzed in the framework of the statistical model code PACE4 [29]. The ICF strength function  $F_{\text{ICF}}$ , which is a measure of the relative strength of ICF to the total fusion cross section, has been deduced and then used for the comparative study with the available literature on same target by different projectiles in terms of different entrance channel parameters. The dependence of incomplete fusion fraction with projectile energy has also been discussed. The purpose of this paper focuses on correlation between the entrance channel parameters and the incomplete fusion fraction. The present results for the above-mentioned system are reported here. The rest of this paper is organized as follows: The experimental methodology and data reduction procedure are given in Sec. II, whereas Sec. III

deals with the results and their interpretations in context with statistical model code PACE4. The influence of ICF on CF and its dependence on various entrance channel parameters is demonstrated in Sec. IV. Finally, a summary and conclusions of this paper are given in Sec. V.

## II. EXPERIMENTAL METHODOLOGY

The present experiments have been performed by utilizing the 15UD Pelletron accelerator facility at the Inter-University Accelerator Center (IUAC), New Delhi (India). Detailed descriptions of the experimental technique and setup are presented in Refs. [7,8], and only a brief description is given here for ready reference. In order to cover a wide energy range for measuring the excitation functions as well as to lower the uncertainty in beam energy, each type of target was grouped in the form of stacks (each stack contains ten target + aluminum foils). Two stacks of  $^{93}\text{Nb}$  targets having thicknesses in the range of 1.2–1.6 mg/cm<sup>2</sup> have been irradiated by  $^{13}\text{C}^{6+}$  beam at energies  $\approx 88$  and 80 MeV. The  $^{93}\text{Nb}$  target foils backed by aluminum (Al) foils thickness from 1.1–1.4 mg/cm<sup>2</sup> have been prepared at the Target Development Laboratory of IUAC, New Delhi, by employing the rolling technique. The Al backing was originally designed for the purpose of the catcher foil to trap the recoiling residues produced in the  $^{13}\text{C} + ^{93}\text{Nb}$  system. To minimize the error in the thickness measurement, the thickness of both  $^{93}\text{Nb}$  target foils as well as aluminum foils has been verified by using the  $\alpha$ -transmission method as well as by the weighing method. Al-catcher foils of sufficient thickness have been placed behind the target foil to completely stop all the evaporation residues. These foils have also worked as an energy degrader to cover the desired energy range. According to the available beam intensity and the expected number of events for each channel, the two stacks have been separately irradiated for about  $\approx 6$  to 7 h in the general purpose scattering chamber. An in-vacuum transfer facility has been used to minimize the time lapse between the stop of irradiation and the beginning of counting. The beam flux has been determined from the charge collected in the Faraday cup installed after the targets by employing a precise current integrator device. The beam current has maintained  $\approx 30\text{--}35$  nA during all the irradiations. The projectile energy on each target foil has been estimated by using the stopping and range of ions in matter code [30].

After irradiation, the activated targets along with catchers have been measured by using precalibrated high-purity germanium (HPGe) detector coupled with the computer automated measurement and control-based data-acquisition system CANDLE [31] software. The Ge crystal (a part of the detector) was surrounded by the lead bricks of 12-cm thickness to reduce background from natural radioactivity. The absolute efficiency of the detector has been determined by using a set of standard radioactive sources ( $^{133}\text{Ba}$  and  $^{152}\text{Eu}$ ) placed in ahead of the HPGe detector. The radioactive sources and the targets are counted in the same geometry. The  $\gamma$ -ray spectrum recorded for the  $^{13}\text{C} + ^{93}\text{Nb}$  system at  $E_{\text{Lab}} = 82.8 \pm 1.1$  MeV is shown in Fig. 1. The evaporation residues are identified not only by their characteristic  $\gamma$ -ray energies, but also by their decay profile. The list of all identified ERs, their

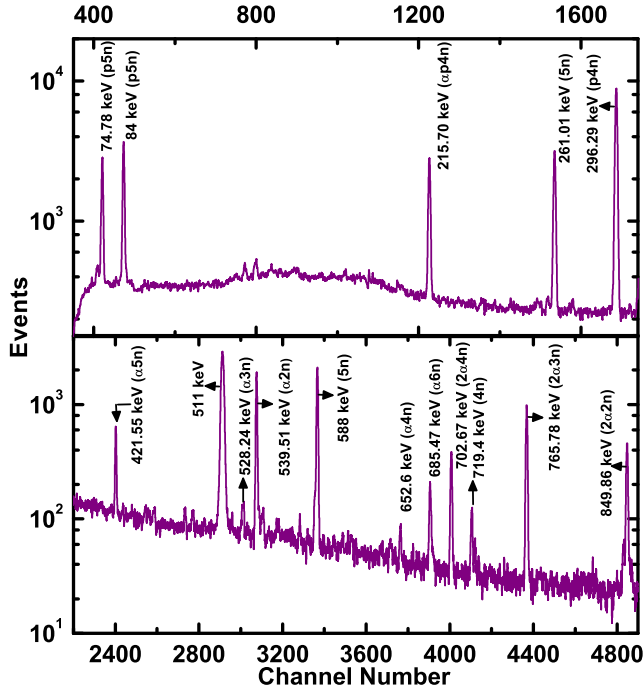


FIG. 1. Typical  $\gamma$ -ray energy spectrum obtained from the interaction of  $^{13}\text{C} + ^{93}\text{Nb}$  system at  $E_{\text{Lab}} = 82.8\text{-MeV}$  energy. Some of the identified  $\gamma$ -ray peaks have been assigned to respective evaporation residues populated via CF and/or ICF channels.

half-lives, and other spectroscopic properties are tabulated in Table I. The nuclear spectroscopic data utilized in the evaluation and the measurements of cross sections have been taken from the Table of Radioactive Isotopes [32]. In order to get comprehensive information about the formation process of the specific reaction products, the cross sections have been computed using the standard formulation [3],

$$\sigma(E) = \frac{A\lambda \exp(\lambda t_2)}{N_0\phi\epsilon_G\theta K[1 - \exp(-\lambda t_1)][1 - \exp(-\lambda t_3)]},$$

where  $A$  is the total number of counts recorded under the peak in time  $t_3$ ,  $N_0$  is the number of target nuclei,  $\phi$  is the incident flux,  $t_1$  is the irradiation time,  $t_2$  is the time lapsed between the stop of irradiation and the start of counting,  $t_3$  is the counting time,  $\theta$  is the branching ratio,  $\lambda$  is the decay constant of the evaporation residue,  $\epsilon_G$  is the geometry-dependent efficiency of the HPGe detector, and  $K$  is the self-absorption correction factor of the  $\gamma$  ray in the target. The C++ program EXPSIGMA designed on the above formulation has been used for calculating the cross section of the ERs. Various factors may be responsible to evoke the errors and uncertainties in the measured cross sections such as: (a) Inaccuracy in the determination of the foil thickness may lead to the uncertainty in calculating the number of target nuclei. Although, it is difficult to know the uncertainty in the target thickness, however, to find the uniformity of the sample, the thickness

TABLE I. List of identified reaction residues in the  $^{13}\text{C} + ^{93}\text{Nb}$  system and their decay data.

Residue	Spin ( $J^P$ )	Half-life ( $T_{1/2}$ )	$E_\gamma$ (keV)	$I_\gamma$ (%)	Reaction channel
$^{102}\text{Ag}$	$5^+$	12.9 min	719.40	54.53	$^{93}\text{Nb}(^{13}\text{C}, 4n)$
$^{101}\text{Ag}$	$9/2^+$	11.1 min	261.01	52.60	$^{93}\text{Nb}(^{13}\text{C}, 5n)$
			588.00	10.00	
$^{101}\text{Pd}$	$5/2^+$	8.47 h	296.29	19.20	$^{93}\text{Nb}(^{13}\text{C}, p4n)$
$^{100}\text{Pd}$	$0^+$	3.63 d	84.00	52.00	$^{93}\text{Nb}(^{13}\text{C}, p5n)$
			74.78	48.00	
$^{100g}\text{Rh}$	$1^-$	20.8 h	539.51	80.60	$^{93}\text{Nb}(^{13}\text{C}, 2p4n)$
					$^{93}\text{Nb}(^{13}\text{C}, \alpha 2n)$
$^{99}\text{Rh}$	$1/2^-$	16.1 d	528.24	37.90	$^{93}\text{Nb}(^{13}\text{C}, 2p5n)$
					$^{93}\text{Nb}(^{13}\text{C}, \alpha 3n)$
$^{98}\text{Rh}$	$2^+$	8.72 min	652.60	97.00	$^{93}\text{Nb}(^{13}\text{C}, 2p6n)$
					$^{93}\text{Nb}(^{13}\text{C}, \alpha 4n)$
$^{97}\text{Rh}$	$9/2^+$	30.7 min	421.55	74.63	$^{93}\text{Nb}(^{13}\text{C}, 2p7n)$
					$^{93}\text{Nb}(^{13}\text{C}, \alpha 5n)$
$^{96}\text{Rh}$	$6^+$	9.90 min	685.47	95.70	$^{93}\text{Nb}(^{13}\text{C}, 2p8n)$
					$^{93}\text{Nb}(^{13}\text{C}, \alpha 6n)$
$^{97}\text{Ru}$	$5/2^+$	2.83 d	215.70	85.62	$^{93}\text{Nb}(^{13}\text{C}, 3p6n)$
					$^{93}\text{Nb}(^{13}\text{C}, \alpha p4n)$
$^{96}\text{Tc}$	$7^+$	4.28 d	849.86	8.00	$^{93}\text{Nb}(^{13}\text{C}, 4p6n)$
					$^{93}\text{Nb}(^{13}\text{C}, \alpha 2p4n)$
					$^{93}\text{Nb}(^{13}\text{C}, 2\alpha 2n)$
$^{95}\text{Tc}$	$9/2^+$	20 h	765.78	93.80	$^{93}\text{Nb}(^{13}\text{C}, 4p7n)$
					$^{93}\text{Nb}(^{13}\text{C}, \alpha 2p5n)$
					$^{93}\text{Nb}(^{13}\text{C}, 2\alpha 3n)$
$^{94}\text{Tc}$	$7^+$	293 min	702.67	99.60	$^{93}\text{Nb}(^{13}\text{C}, 4p8n)$
					$^{93}\text{Nb}(^{13}\text{C}, \alpha 2p6n)$
					$^{93}\text{Nb}(^{13}\text{C}, 2\alpha 4n)$

of each target foil has been measured at various positions by the  $\alpha$ -transmission method as well as by the weighing method. Presently, the error in the thickness of the target foils comes out to be  $<2\%$ . (b) The fluctuations in the beam current during the irradiation may result in the variation of incident flux. Proper care has been taken to keep the beam current constant, and the error due to beam fluctuation is estimated to be  $<6\%$ . (c) The uncertainty in the determination of geometry-dependent efficiency may also add to some error in the measured cross sections. (d) The dead time of the spectrometer may also lead to the error. The dead time was kept  $<10\%$  by adjusting the distance between the irradiated foils and the detector. Attempts were made to minimize the uncertainties caused by all the above factors. Apart from the uncertainties in the decay constant and branching ratio, the overall errors including statistical errors in the present measurements are estimated to be  $\leq 15\%$ .

### III. OBTAINED RESULTS, ANALYSIS, AND THEIR INTERPRETATION

The excitation functions for 13 evaporation residues, namely,  $^{102}\text{Ag}(4n)$ ,  $^{101}\text{Ag}(5n)$ ,  $^{101}\text{Pd}(p4n)$ ,  $^{100}\text{Pd}(p5n)$ ,  $^{100g}\text{Rh}(\alpha 2n)$ ,  $^{99}\text{Rh}(\alpha 3n)$ ,  $^{98}\text{Rh}(\alpha 4n)$ ,  $^{97}\text{Rh}(\alpha 5n)$ ,  $^{96}\text{Rh}(\alpha 6n)$ ,  $^{97}\text{Ru}(\alpha 4n)$ ,  $^{96}\text{Tc}(2\alpha 2n)$ ,  $^{95}\text{Tc}(2\alpha 3n)$ , and  $^{94}\text{Tc}(2\alpha 4n)$  produced in the  $^{13}\text{C} + ^{93}\text{Nb}$  system have been measured. These measured excitation functions have been analyzed by employing the statistical model code PACE4 [29], which takes under consideration only the CF contribution. This code is based on the Hauser-Feshbach theory of CN decay [33]. In this code, at each stage of deexcitation the angular momentum projections are calculated, which enables the determination of angular distributions of emitted particles, and angular momentum conservation is explicitly taken into account. The CF cross sections have been calculated using the Bass formula [34]. For the CN formation, the partial cross section ( $\sigma_\ell$ ) related to the individual angular momentum ( $\ell$ ) values at a particular incident energy is given by

$$\sigma_\ell = \pi \tilde{\lambda}^2 (2\ell + 1) T_\ell,$$

where  $\tilde{\lambda}$  is the reduced wavelength and the transmission coefficient ( $T_\ell$ ) is taken to be

$$T_\ell = \left[ 1 + \exp\left(\frac{\ell - \ell_{\max}}{\Delta}\right) \right]^{-1},$$

where  $\Delta$  is the diffuseness parameter and  $\ell_{\max}$  is maximum value of  $\ell$  detained by the total CF cross section,

$$\sigma_{\text{CF}} = \sum_{\ell}^{\infty} \sigma_\ell.$$

The transmission coefficient for light emitted particles, such as neutron ( $n$ ), proton ( $p$ ), and  $\alpha$  ( $\alpha$ ) are calculated using the optical model potentials [35]. Gilbert and Camerons level-density parameter value was used during the calculations [36]. In this code, level-density parameter ( $a = A/K \text{ MeV}^{-1}$ , where  $A$  is the mass number of the CN and  $K$  is a free parameter) is one of the important parameters in the PACE4 code. The different values of  $K$  (8, 10, 12) have been tested

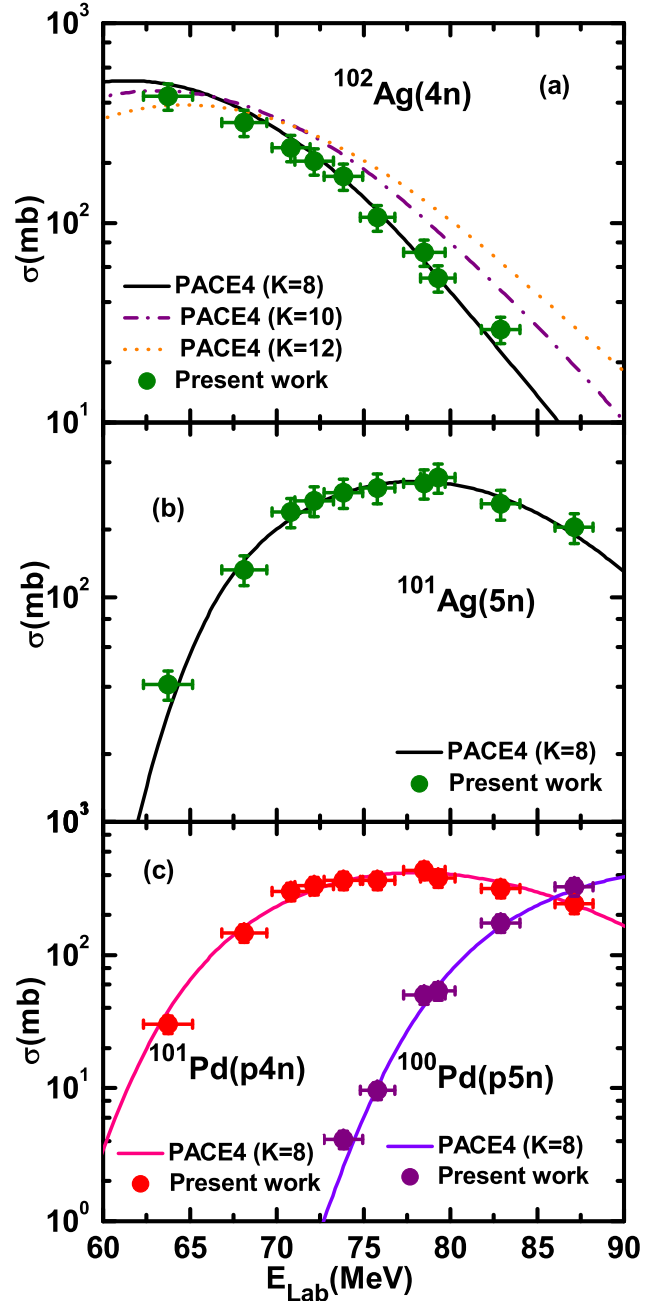


FIG. 2. (a) Experimentally measured EFs of evaporation residue  $^{102}\text{Ag}(4n)$  along with PACE4 calculations ( $K = 8, 10, \text{ and } 12$ ). (b) Experimentally measured EFs of evaporation residues  $^{101}\text{Ag}(5n)$  along with PACE4 calculations ( $K = 8$ ). (c) Experimentally measured EFs of evaporation residues  $^{101}\text{Pd}(p4n)$  and  $^{100}\text{Pd}(p5n)$  along with PACE4 calculations ( $K = 8$ ).

to match the experimental data. As a representative case, the effect of variation of the parameter  $K$  on calculated EFs of residue  $^{102}\text{Ag}$  populated via  $4n$  is presented in Fig. 2(a). A value of  $K = 8$  is found to be a physically suitable value to reproduce the measured EFs data of all complete fusion channels satisfactorily. Measured cross-section data are presented in Table II. The evaporation residues produced through vari-

TABLE II. Experimentally measured production reaction cross-sections  $\sigma$  (mb) of identified evaporation residues in the  $^{13}\text{C} + ^{93}\text{Nb}$  system.

$E_{\text{Lab}}$ (MeV)	$\sigma(^{102}\text{Ag})$ (mb)	$\sigma(^{101}\text{Ag})$ (mb)	$\sigma(^{101}\text{Pd})$ (mb)	$\sigma(^{100}\text{Pd})$ (mb)	$\sigma(^{100\text{g}}\text{Rh})$ (mb)	$\sigma(^{99}\text{Rh})$ (mb)	$\sigma(^{98}\text{Rh})$ (mb)
87.1 ± 1.1	8.6 ± 1.2	204.6 ± 30.6	241.5 ± 36.2	325.5 ± 48.8	71.6 ± 10.7		197.3 ± 21.7
82.8 ± 1.1	29.3 ± 4.3	260.0 ± 39.0	316.5 ± 47.4	174.2 ± 26.1	36.6 ± 5.4	29.4 ± 3.5	235.4 ± 25.9
79.2 ± 1.0	53.0 ± 7.9	341.5 ± 51.2	379.1 ± 56.8	53.9 ± 8.0	13.6 ± 2.0	49.4 ± 5.9	231.5 ± 25.4
78.5 ± 1.2	71.1 ± 10.6	321.0 ± 48.1	433.9 ± 65.0	49.9 ± 7.4	10.5 ± 1.5	53.6 ± 6.4	223.2 ± 24.5
75.8 ± 1.0	106.4 ± 15.9	307.1 ± 46.0	363.6 ± 54.5	9.6 ± 1.4	6.7 ± 1.0	88.8 ± 10.6	185.8 ± 20.4
73.8 ± 1.1	170.6 ± 25.6	292.4 ± 43.8	363.4 ± 54.5	4.1 ± 0.6	8.4 ± 1.2	110.9 ± 13.3	142.4 ± 15.6
72.1 ± 1.1	204.2 ± 30.6	269.2 ± 40.3	332.3 ± 49.8		10.2 ± 1.5	122.3 ± 14.6	117.7 ± 12.2
70.8 ± 1.0	238.0 ± 35.7	239.8 ± 35.9	301.5 ± 45.2		11.4 ± 1.7	128.8 ± 15.4	89.4 ± 9.8
68.1 ± 1.3	317.9 ± 47.6	132.6 ± 19.8	142.6 ± 21.9		13.4 ± 2.0	150.8 ± 18.0	44.5 ± 4.8
63.7 ± 1.4	430.4 ± 64.5	40.8 ± 6.1	30.2 ± 4.5		22.1 ± 3.3	149.2 ± 17.9	
$E_{\text{Lab}}$ (MeV)	$\sigma(^{97}\text{Rh})$ (mb)	$\sigma(^{96}\text{Rh})$ (mb)	$\sigma^{\text{ind}}(^{97}\text{Ru})$ (mb)	$\sigma(^{96}\text{Tc})$ (mb)	$\sigma(^{95}\text{Tc})$ (mb)	$\sigma(^{94}\text{Tc})$ (mb)	
87.1 ± 1.1	107.8 ± 18.3	12.4 ± 1.8	86.6 ± 12.9		53.5 ± 8.0	19.8 ± 2.9	
82.8 ± 1.1	45.7 ± 7.7	8.3 ± 1.2	24.6 ± 3.6	17.4 ± 2.6	48.6 ± 7.2	6.3 ± 0.9	
79.2 ± 1.0	6.9 ± 1.1	6.6 ± 1.0	12.8 ± 1.9	18.2 ± 2.7	42.5 ± 6.3	2.2 ± 0.3	
78.5 ± 1.2	4.5 ± 0.7	6.0 ± 0.9	8.8 ± 1.3	18.8 ± 2.8	40.4 ± 6.0	1.2 ± 0.1	
75.8 ± 1.0		4.0 ± 0.6	4.7 ± 0.7	20.8 ± 3.1	31.3 ± 4.6		
73.8 ± 1.1		3.0 ± 0.4		21.7 ± 3.2	20.5 ± 3.0		
72.1 ± 1.1				19.1 ± 2.8	10.6 ± 1.5		
70.8 ± 1.0				17.6 ± 2.6	8.4 ± 1.2		
68.1 ± 1.3				15.2 ± 2.2	2.9 ± 0.4		
63.7 ± 1.4				10.1 ± 1.5			

ous reaction channels in the  $^{13}\text{C} + ^{93}\text{Nb}$  system are discussed below.

### A. Excitation function measurement of $xn$ and $pxn$ emitting channels

The experimentally measured EFs of residues  $^{102}\text{Ag}(4n)$ ,  $^{101}\text{Ag}(5n)$ ,  $^{101}\text{Pd}(p4n)$ , and  $^{100}\text{Pd}(p5n)$  populated in the  $^{13}\text{C} + ^{93}\text{Nb}$  system are displayed in Figs. 2(a)–2(c), respectively. In the present paper a value of  $K = 8$  is found to nicely reproduce the measured EFs data of residue  $^{102}\text{Ag}$  when compared with PACE4 predictions estimated for  $K = 8, 10$ , and  $12$ . As such, the value of  $K = 8$  is additionally found to be suitable for best fit with the measured data for all the  $xn$  and/or  $pxn$  emission channels. It can be seen from Fig. 2 that the measured cross sections of ERs  $^{102}\text{Ag}$ ,  $^{101}\text{Ag}$ ,  $^{101}\text{Pd}$ , and  $^{100}\text{Pd}$  are satisfactorily reproduced with theoretical predictions of PACE4 over the studied range of energy. Since the PACE4 calculations are based on compound nucleus theory and do not take the ICF under consideration, it is evident that these evaporation residues are formed by deexcitation of compound nucleus  $^{106}\text{Ag}^*$  via  $xn$  and/or  $pxn$  channels.

### B. Excitation function measurement for the $\alpha xn$ , $\alpha pxn$ , and $2\alpha xn$ emitting channels

The experimentally measured EFs of residues  $^{100\text{g}}\text{Rh}(\alpha 2n)$ ,  $^{99}\text{Rh}(\alpha 3n)$ ,  $^{98}\text{Rh}(\alpha 4n)$ ,  $^{97}\text{Rh}(\alpha 5n)$ ,  $^{96}\text{Rh}(\alpha 6n)$ ,  $^{97}\text{Ru}(\alpha p4n)$ ,  $^{96}\text{Tc}(2\alpha 2n)$ ,  $^{95}\text{Tc}(2\alpha 3n)$ , and  $^{94}\text{Tc}(2\alpha 4n)$  populated in the

$^{13}\text{C} + ^{93}\text{Nb}$  system are shown in Figs. 3 and 4. The experimentally measured cross sections for these ERs have been compared with the theoretical predictions of PACE4. The PACE4 calculations have been performed with the same set of input parameters, which have been used to reproduce the EFs of  $xn$  and/or  $pxn$  channels produced via the CF mode. As we already discussed in the previous section, the PACE4 code does not calculate the ICF cross sections, and, thus, if any enhancement in the experimental EFs over the PACE4 predictions may be assigned to the contribution from ICF processes. This implies that these ERs are populated by the ICF process in addition to the CF. From Fig. 3(a), it can be seen that two humps are observed for the excitation functions of  $^{100}\text{Rh}$ . This could be explained as being relatively low threshold energy for  $(\alpha 2n)$  reaction channel the  $^{100}\text{Rh}$  is mainly produced by complete/incomplete fusion of projectile to the target, however, at relatively higher energies, being comparatively much higher threshold value for  $(2p4n)$  reaction channel the residue  $^{100}\text{Rh}$  may also be produced through this route.

During the decay-curve analysis, the evaporation residue  $^{97}\text{Ru}$  ( $t_{1/2} = 2.83$  d) populated through the emission of  $(\alpha p4n)$  channel is strongly fed from its precursor  $^{97}\text{Rh}$  ( $t_{1/2} = 30.7$  min). The independent cross-sections ( $\sigma_{\text{ind}}$ ) have been estimated from the cumulative cross-sections ( $\sigma_{\text{cum}}$ ) by using the Cavinato *et al.* [37] formulation given as

$$\sigma_{\text{ind}} = \sigma_{\text{cum}} - P_{\text{pre}} \left[ \frac{t_{1/2}^D}{t_{1/2}^D - t_{1/2}^P} \right] \sigma_P.$$

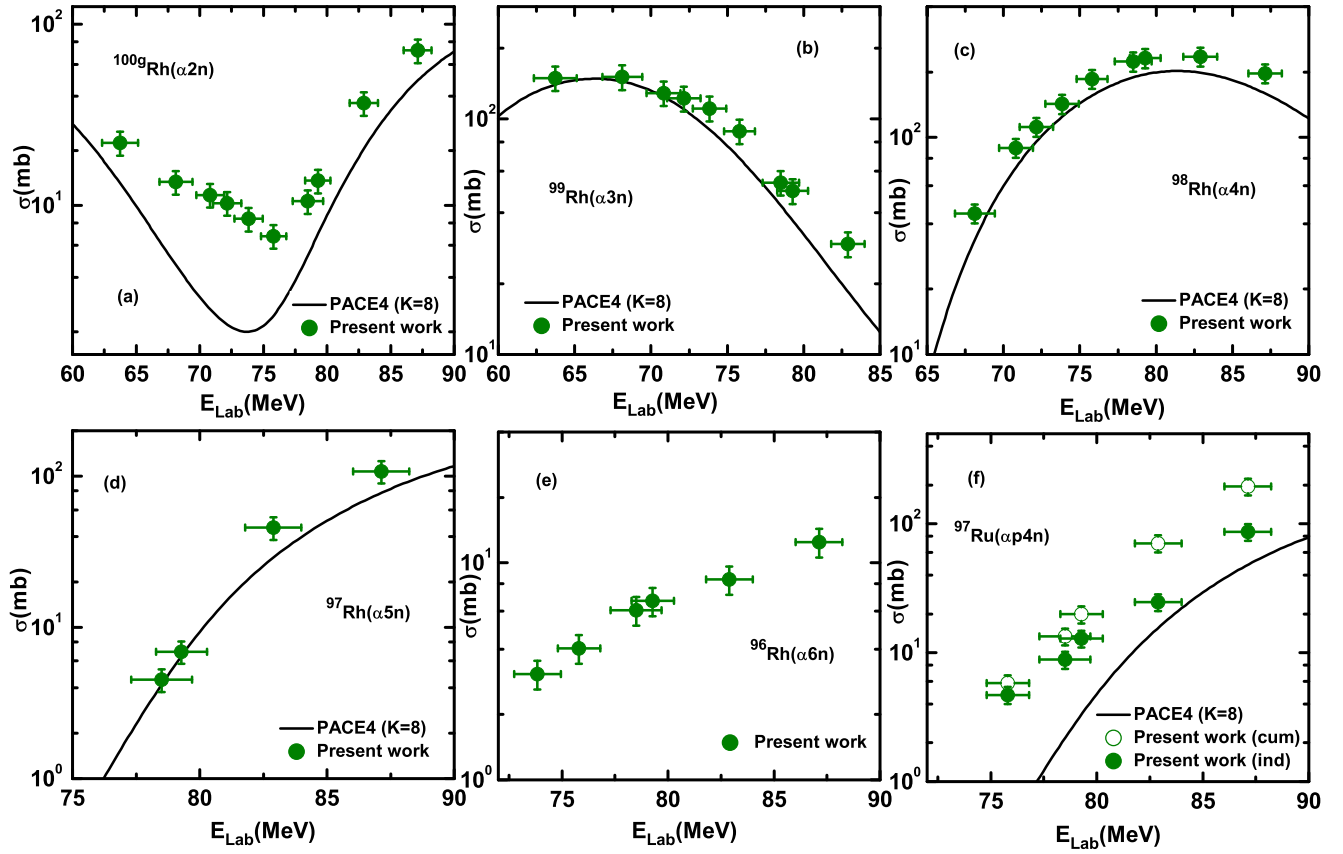


FIG. 3. Experimentally measured EFs of evaporation residues  $^{100g}\text{Rh}(\alpha 2n)$ ,  $^{99}\text{Rh}(\alpha 3n)$ ,  $^{98}\text{Rh}(\alpha 4n)$ ,  $^{97}\text{Rh}(\alpha 5n)$ ,  $^{96}\text{Rh}(\alpha 6n)$ , and  $^{97}\text{Ru}(\alpha p 4n)$  [panels (a)–(f)] are compared with PACE4 predictions ( $K = 8$ ). The hollow symbol represents the measured cumulative cross section. For  $^{100g}\text{Rh}$  the EFs also include the precursor contribution from  $^{100}\text{Pd}$ .

Here  $\sigma_P$  is the cross section of parent nuclei, and  $t_{1/2}^D$  and  $t_{1/2}^P$  are the half-lives of the daughter and precursor nuclei.  $P_{\text{pre}}$  is the branching ratio of the precursor to its daughter nuclei. The independent cross section has been evaluated using the following expression:

$$\sigma_{\text{ind}}^{97\text{Ru}} = \sigma_{\text{cum}}^{97\text{Ru}} - 1.007\sigma_{\text{ind}}^{97\text{Rh}}.$$

Here ( $P_{\text{pre}} = 1$ ) [32]. The values of  $\sigma_{\text{ind}}$  and  $\sigma_{\text{cum}}$  for  $^{97}\text{Ru}(\alpha p 4n)$  are given in Fig. 3(f). The nucleus  $^{100}\text{Rh}(\alpha 2n)$  channel may also have a contribution from its higher charge isobar precursors  $^{100}\text{Pd}$  through their  $\beta$ +/ $\text{EC}$  decay. But the formulation given by Cavinato *et al.* [37] does not hold satisfactorily as the daughter nucleus has a shorter half-life than the parent nucleus. In the present paper, the

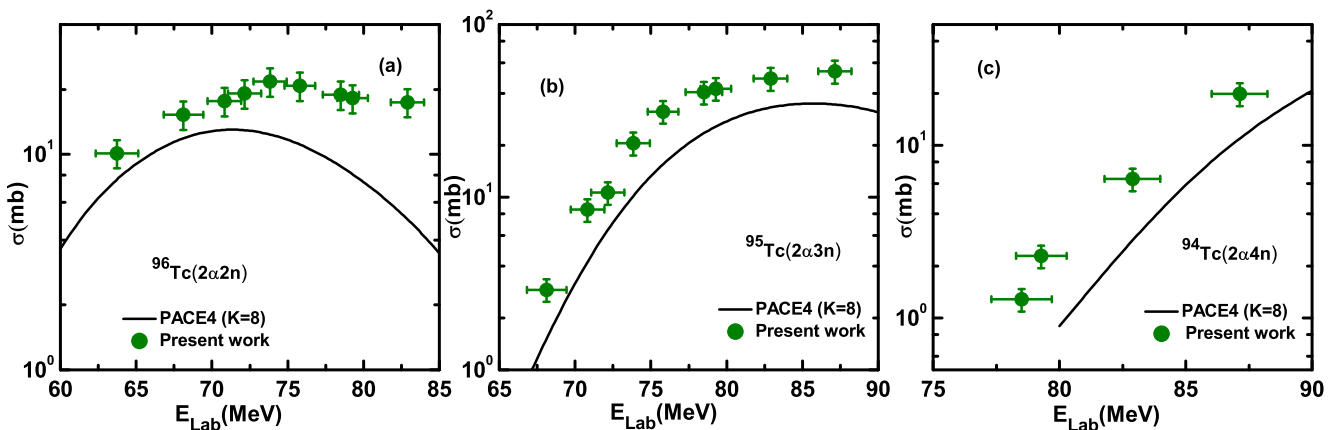
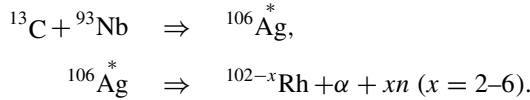


FIG. 4. Experimentally measured EFs of evaporation residues  $^{96}\text{Tc}(2\alpha 2n)$ ,  $^{95}\text{Tc}(2\alpha 3n)$ , and  $^{94}\text{Tc}(2\alpha 4n)$  are compared with PACE4 predictions ( $K = 8$ ).

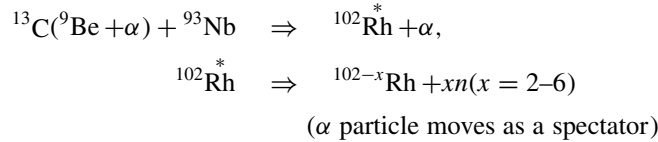
precursor contribution for production of nucleus  $^{100}\text{Rh}$  could not be obtained since the nucleus of  $^{100}\text{Rh}$  has both meta and ground states of half-lives 4.6 min and 20.8 h, respectively. In the present paper, the production of the experimental cross section of  $^{100m}\text{Rh}$  could not be achieved due to the shorter half-life of the residues (4.6 min) as is the experimental limitation of the off-beam activation technique. As a result of this, the production cross section of parent nucleus  $^{100}\text{Pd}$  is larger as compared to the production of daughter nucleus  $^{100}\text{Rh}$ . In such a case, no attempt may be made to extract independent production of the daughter nucleus. Moreover, no contribution from any higher charge isobar has been observed in any other  $\alpha$  or  $2\alpha$  emission channels, hence, their experimentally measured cross sections are independent in nature. As can be seen from Figs. 3 and 4, the experimental EFs of  $^{100g,99,98,97}\text{Rh}$ ,  $^{97}\text{Ru}$ , and  $^{96,95,94}\text{Tc}$  residues show a significant enhancement as compared to the PACE4 calculations. The enhancement in the experimental cross sections for the  $\alpha$ -emitting channels may be attributed to the contribution of the ICF processes at the studied range of energies. The reaction mechanism involved in the formation of ERs populated through  $\alpha$  and  $2\alpha$  emission channels may be represented as

1 $\alpha$ -emission case

(a) CF of  $^{13}\text{C}$  with  $^{93}\text{Nb}$

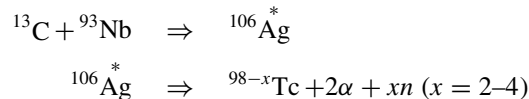


(b) ICF of  $^{13}\text{C}$  with  $^{93}\text{Nb}$ ,

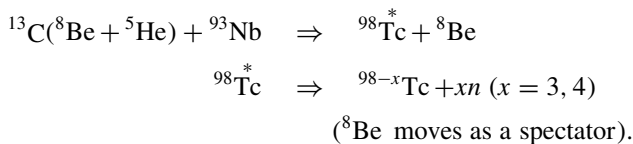


2 $\alpha$ -emission case

(a) CF of  $^{13}\text{C}$  with  $^{93}\text{Nb}$ ,



(b) ICF of  $^{13}\text{C}$  with  $^{93}\text{Nb}$ ,



Here, it is important to note that the theoretical prediction of the PACE4 code gives negligible cross sections as compared to measured cross section for the evaporation residue  $^{96}\text{Rh}$  produced via an  $\alpha 6n$  emission channel and, hence, are not shown in Fig. 3(e), indicating the production of this residue solely via ICF processes.

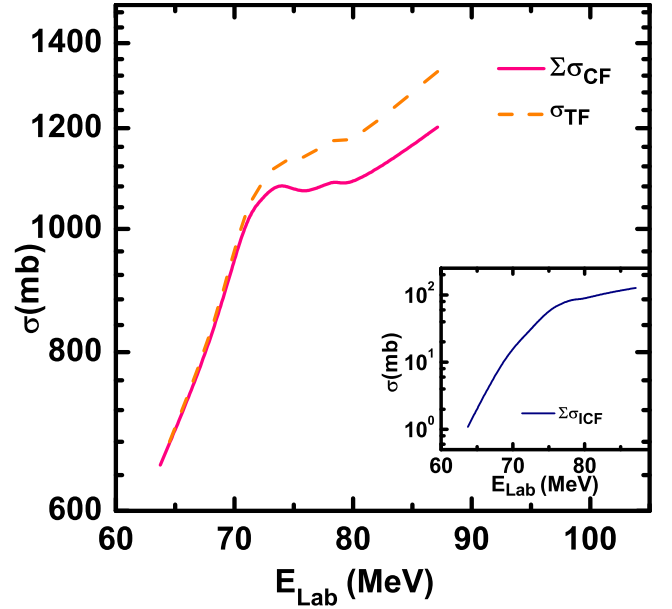


FIG. 5. The total fusion cross-section ( $\sigma_{\text{TF}}$ ) along with the sum of all complete fusion ( $\Sigma\sigma_{\text{CF}}$ ) and in the inset the incomplete fusion cross-section ( $\Sigma\sigma_{\text{ICF}}$ ) is plotted as a function of incident projectile energy.

#### IV. EFFECT OF ENTRANCE CHANNEL PARAMETERS ON ICF

An attempt has been made to deduce the ICF contribution from the analysis of excitation function data and its dependency on various entrance channel parameters, i.e., projectile energy, projectile structure, target, mass asymmetry of interacting partners, and projectile  $Q_\alpha$  value. The role of ICF in the formation of all  $\alpha$  and  $2\alpha$  emitting channels has been studied by calculating  $\Sigma\sigma_{\text{ICF}}$  as  $\Sigma\sigma_{\text{ICF}} = \Sigma\sigma_{\text{Expt.}} - \Sigma\sigma_{\text{PACE4}}$ . So as to extract more information regarding how much incompletely fused channels contribute to the total fusion cross-section ( $\sigma_{\text{TF}} = \Sigma\sigma_{\text{CF}} + \Sigma\sigma_{\text{ICF}}$ ), the sum of CF cross sections of all channels ( $\Sigma\sigma_{\text{CF}}$ ) and  $\sigma_{\text{TF}}$  is plotted against incident projectile energy in Fig. 5. It is clear from this figure that the separation between  $\sigma_{\text{TF}}$  and  $\Sigma\sigma_{\text{CF}}$  continuously increases with an increase in projectile energy, implying the significant ICF contribution along with CF. To get a proper insight into the onset and strength of the ICF, the ICF strength function  $F_{\text{ICF}}$  has been deduced for the present studied system  $^{13}\text{C} + ^{93}\text{Nb}$ . The  $F_{\text{ICF}}(\%)$  is a measurement of strength of the ICF relative to total fusion and is defined as  $F_{\text{ICF}}(\%) = [(\Sigma\sigma_{\text{TF}} - \Sigma\sigma_{\text{PACE4}})/\sigma_{\text{TF}}] \times 100$ . The effect of various entrance channel parameters on the ICF reaction dynamics will be discussed in the following subsections.

##### A. ICF dependence on incident beam energy

To examine the effect of projectile energy on ICF dynamics, the deduced ICF probability [ $F_{\text{ICF}}(\%)$ ] for the present system along with those obtained for projectiles ( $^{16}\text{O}$ ,  $^{18}\text{O}$ )

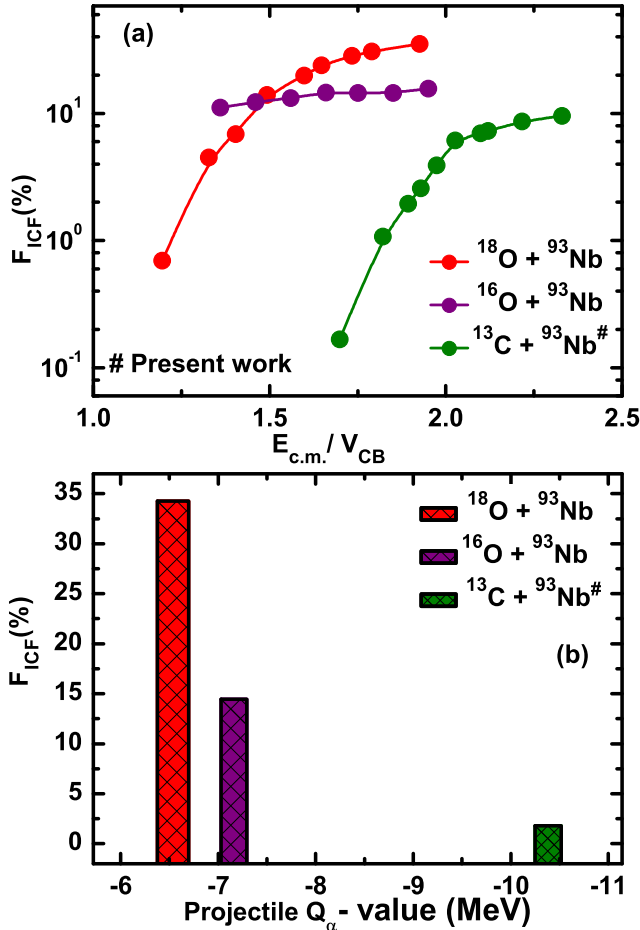


FIG. 6. (a) The comparison of deduced  $F_{ICF}(\%)$  as a function of normalized projectile energy for different projectiles with the same target  $^{93}\text{Nb}$ . (b) Comparison of  $F_{ICF}(\%)$  in terms of the projectile  $Q_\alpha$  value at constant relative velocity ( $V_{rel} = 0.074c$ ) for  $^{13}\text{C}$ ,  $^{16}\text{O}$ , and  $^{18}\text{O}$  projectiles with the same  $^{93}\text{Nb}$  target. For references and details see the text.

on the same target  $^{93}\text{Nb}$  has been plotted as a function of normalized projectile energy and is shown in Fig. 6(a). The energy axis has been normalized by Coulomb barrier ( $V_{CB}$ ) to wash out the Coulomb barrier effect for presently studied projectile-target combinations. This figure clearly shows that  $F_{ICF}(\%)$ , in general, increases with normalized projectile energy for all the systems studied. As shown in Fig. 6(a), the value of  $F_{ICF}(\%)$  increases continuously from 0.16% to 9.57% at the highest measured energy in the  $^{13}\text{C} + ^{93}\text{Nb}$  system. A similar increase in  $F_{ICF}(\%)$  is also found for the system of  $^{16}\text{O} + ^{93}\text{Nb}$  [38] and  $^{18}\text{O} + ^{93}\text{Nb}$  [39] systems with an increase in the incident energy. Furthermore, it is clearly indicated that the projectile breakup probability increases with an increase in the projectile energy and may be reflected in the influence of input angular momentum. From this figure, it can also be noted that the ICF contribution for  $^{18}\text{O}$  and  $^{16}\text{O}$  is larger than that of the  $^{13}\text{C}$  projectile. Hence, the present results indicated that the projectile structure effect also plays a crucial role on the ICF probability.

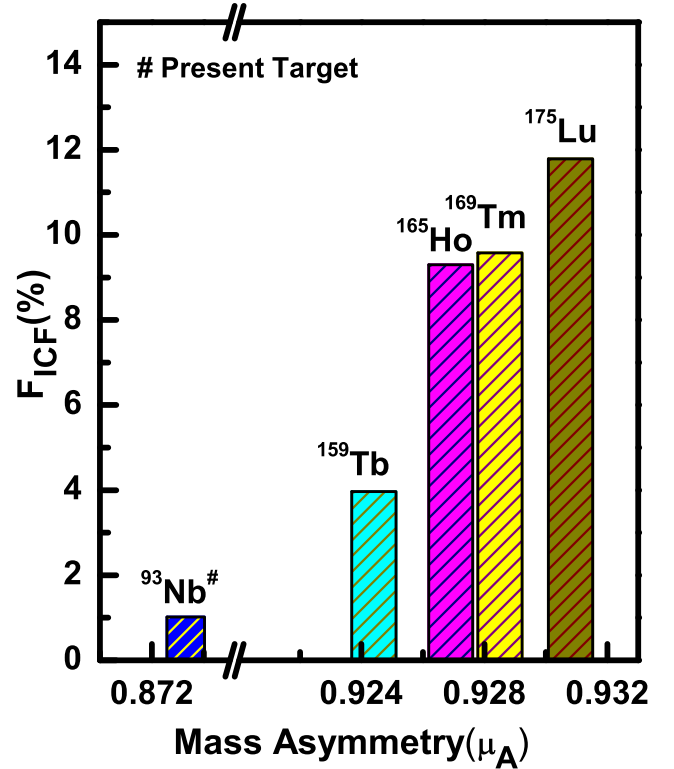


FIG. 7. Comparison of deduced  $F_{ICF}(\%)$  for the  $^{13}\text{C}$ -induced reaction with  $^{93}\text{Nb}$ ,  $^{159}\text{Tb}$ ,  $^{165}\text{Ho}$ ,  $^{169}\text{Tm}$ , and  $^{175}\text{Lu}$  targets as a function of mass-asymmetry [ $\mu_A = A_T/(A_T + A_P)$ ] at constant relative velocity ( $V_{rel} = 0.071c$ ). For references and details see the text.

### B. ICF dependence on mass-asymmetry ( $\mu_A$ )

In this subsection, we will discuss how the ICF probability depends upon mass asymmetry of interacting partners. As pointed out earlier that Morgenstern *et al.* [26] suggested that the mass asymmetry between the interacting partners influences the ICF probability at the constant relative velocity, which was further supported by some other studies [27,40]. The relative velocity ( $V_{rel}$ ) between the interacting partners is defined as  $V_{rel} = \sqrt{2(E_{c.m.} - V_{CB})/\mu}$ , where  $E_{c.m.}$  is the projectile energy in the center-of-mass frame,  $\mu$  is the reduced mass of the system, and  $V_{CB}$  is the Coulomb barrier between two interacting partners. The mass asymmetry of the interacting partners is given as  $\mu_A = A_T/(A_T + A_P)$ , where  $A_T$  is the mass of the target and  $A_P$  is the mass of the projectile. The values of  $F_{ICF}(\%)$  for the present  $^{13}\text{C} + ^{93}\text{Nb}$  system have been compared with those obtained for  $^{13}\text{C} + ^{159}\text{Tb}$  [9],  $^{13}\text{C} + ^{165}\text{Ho}$  [41],  $^{13}\text{C} + ^{169}\text{Tm}$  [42], and  $^{13}\text{C} + ^{175}\text{Lu}$  [43] systems at a normalized relative velocity ( $V_{rel} = 0.071c$ ) as a function of entrance channel mass asymmetry and presented in Fig. 7. This figure clearly indicates that ICF probability [ $F_{ICF}(\%)$ ] depends strongly on mass asymmetry of the interacting system and increases with an increase in entrance channel mass asymmetry.



### C. ICF dependence on projectile $Q_\alpha$ value

In this subsection, the role of projectile structure can be studied as one of the influenceable observables in terms of projectile  $Q_\alpha$  value systematic. The projectile  $Q_\alpha$  value simply determines the quantity of energy required in separating the  $\alpha$  particle from the projectile, which is often also termed as projectile  $\alpha$ -separation energy. So as to look at the  $Q_\alpha$  value systematic in more clear way, the  $F_{\text{ICF}}(\%)$  for the presently studied system  $^{13}\text{C} + ^{93}\text{Nb}$  system have been compared with those obtained for  $^{16}\text{O} + ^{93}\text{Nb}$  [38] and  $^{18}\text{O} + ^{93}\text{Nb}$  [39] systems at a constant relative velocity ( $V_{\text{rel}} = 0.071c$ ) as a function of the projectile  $Q_\alpha$  value and is plotted in Fig. 6(b). This figure clearly shows that ICF probability is higher for projectile  $^{18}\text{O}$  in comparison to the other projectiles  $^{16}\text{O}$  and  $^{13}\text{C}$ . The  $Q_\alpha$  values for projectiles  $^{18}\text{O}$ ,  $^{16}\text{O}$ , and  $^{13}\text{C}$  are as follows:

$$\begin{aligned} ^{18}\text{O} &\Rightarrow ^{14}\text{C} + \alpha, & Q_\alpha &= -6.22 \text{ MeV}, \\ ^{16}\text{O} &\Rightarrow ^{12}\text{C} + \alpha, & Q_\alpha &= -7.16 \text{ MeV}, \\ ^{13}\text{C} &\Rightarrow ^9\text{Be} + \alpha, & Q_\alpha &= -10.65 \text{ MeV}. \end{aligned}$$

From the data presented in Fig. 6(b), it can be seen that the value of  $F_{\text{ICF}}(\%)$  is found to be more for a less than a negative  $Q_\alpha$  value for a projectile than a more negative  $Q_\alpha$  value projectile. Present findings well support the previous findings [7,9,22], and it can be concluded that the  $Q_\alpha$  value is important for the study of ICF reaction dynamics.

### V. SUMMARY AND CONCLUSION

To probe the correlation between the entrance channel parameters and the ICF fraction on incomplete fusion dynamics, excitation functions for the assembly of the radionuclides  $^{102}\text{Ag}(4n)$ ,  $^{101}\text{Ag}(5n)$ ,  $^{101}\text{Pd}(p4n)$ ,  $^{100}\text{Pd}(p5n)$ ,  $^{100g}\text{Rh}(\alpha 2n)$ ,  $^{99}\text{Rh}(\alpha 3n)$ ,  $^{98}\text{Rh}(\alpha 4n)$ ,  $^{97}\text{Rh}(\alpha 5n)$ ,  $^{96}\text{Rh}(\alpha 6n)$ ,  $^{97}\text{Ru}(\alpha p4n)$ ,  $^{96}\text{Tc}(2\alpha 2n)$ ,  $^{95}\text{Tc}(2\alpha 3n)$ , and  $^{94}\text{Tc}(2\alpha 4n)$  have been measured in the energy range of 63.7–87.1 MeV for the  $^{13}\text{C} + ^{93}\text{Nb}$  system. During the decay curve analysis, it has

been found one of the  $(\alpha p4n)$  channels fed by their higher charge precursor isobar and has also been calculated using the formalism of Cavinato *et al.* [37]. The experimentally measured cross sections of the ERs populated via  $xn$  and/or  $pxn$  channels have been found to be in good agreement with the theoretical predictions of statistical model code PACE4 for level-density parameter  $a = A/8 \text{ MeV}^{-1}$  over the studied energy range. However, in the case of  $\alpha$ -emitting channels, the observed enhancement of cross sections over the predictions of statistical model calculations may be assigned to the ICF process. Furthermore, in order to achieve a better understanding the role of various entrance channel parameters, the values of an incomplete fusion fraction for some other systems taken from literature are compared. On the basis of analysis and results presented in this paper, it may be concluded that the ICF strongly depends on incident energy, mass asymmetry, primary structure of the projectile and target, and projectile  $Q_\alpha$  value. Results and analysis presented on projectile structure effects suggest more ICF fraction for the less negative projectile  $Q_\alpha$  value. The results obtained from the excitation functions are quite interesting, new, and give fruitful information for establishing the complete and incomplete fusions at relatively low bombarding energies.

### ACKNOWLEDGMENTS

We were thankful to the Director IUAC, New Delhi for providing all the necessary facilities to carry out the experiment. A.A. was thankful to the Science and Engineering Research Board (SERB), Department of Science and Technology (DST), New Delhi, India for financial support through Research Project No. EMR/2016/006983. Thanks are also due to Dr. Manoj K. Sharma for carefully reading the paper and giving valuable suggestions. We also extend our gratitude towards Dr. V. P. Singh, Head Physics Department and Dr. Anuraag Mohan Principal, Bareilly College, Bareilly (India) for their support and interest in this paper. Thanks also are due to Target Laboratory especially Abhilash S. R., and the technical staff of Pelletron Laboratory for providing the uninterrupted and stable beam during the experiment.

- 
- [1] D. Kumar, M. Maiti, and S. Lahiri, *Phys. Rev. C* **96**, 014617 (2017).
- [2] M. Gull, K. Kumar, S. Ali, T. Ahmad, S. Dutt, I. A. Rizvi, A. Agarwal, and R. Kumar, *Phys. Rev. C* **98**, 034603 (2018).
- [3] A. Agarwal, I. A. Rizvi, R. Kumar, B. K. Yogi, and A. K. Chaubey, *Int. J. Mod. Phys. E* **17**, 393 (2008).
- [4] R. Prajapat and M. Maiti, *Phys. Rev. C* **101**, 024608 (2020).
- [5] N. T. Zhang, Y. D. Fang, P. R. S. Gomes, J. Lubian, M. L. Liu, X. H. Zhou, G. S. Li, J. G. Wang, S. Guo, Y. H. Qiang, Y. H. Zhang, D. R. Mendes Junior, Y. Zheng, X. G. Lei, B. S. Gao, Z. G. Wang, K. L. Wang, and X. F. He, *Phys. Rev. C* **90**, 024621 (2014).
- [6] K. Kumar, T. Ahmad, S. Ali, I. A. Rizvi, A. Agarwal, R. Kumar, and A. K. Chaubey, *Phys. Rev. C* **88**, 064613 (2013).
- [7] K. Kumar, T. Ahmad, S. Ali, I. A. Rizvi, A. Agarwal, R. Kumar, K. S. Golda, and A. K. Chaubey, *Phys. Rev. C* **87**, 044608 (2013).
- [8] A. Yadav, V. R. Sharma, P. P. Singh, D. P. Singh, M. K. Sharma, U. Gupta, R. Kumar, B. P. Singh, R. Prasad, and R. K. Bhowmik, *Phys. Rev. C* **85**, 034614 (2012).
- [9] A. Yadav, V. R. Sharma, P. P. Singh, R. Kumar, D. P. Singh Unnati, M. K. Sharma, B. P. Singh, and R. Prasad, *Phys. Rev. C* **86**, 014603 (2012).
- [10] F. K. Amanuel, B. Zelalem, A. K. Chaubey, A. Agarwal, I. A. Rizvi, A. Maheshwari, and T. Ahmed, *Phys. Rev. C* **84**, 024614 (2011).
- [11] H. C. Britt and A. R. Quinon, *Phys. Rev.* **124**, 877 (1961).
- [12] T. Udagawa and T. Tamura, *Phys. Rev. Lett.* **45**, 1311 (1980).
- [13] J. Wilczynski, K. Siwek-Wilczynska, J. Van-Driel, S. Gonggrijp, D. C. J. M. Hageman, R. V. F. Janssens, J. Lukasiak, R. H. Siemssen, and S. Y. Van Der Werf, *Nucl. Phys.* **A373**, 109 (1982).
- [14] J. P. Bondroff, J. N. De, G. Fai, A. O. T. Karvinen, and J. Randrup, *Nucl. Phys.* **A333**, 285 (1980).

- [15] M. Blann, *Phys. Rev. C* **31**, 295(R) (1985).
- [16] R. Weiner and M. Westrom, *Nucl. Phys.* **A286**, 282 (1977).
- [17] I. Tserruya, V. Steiner, Z. Fraenkel, P. Jacobs, D. G. Kovar, W. Henning, M. F. Vineyard, and B. G. Glagola, *Phys. Rev. Lett.* **60**, 14 (1988).
- [18] D. J. Parker, J. J. Hogan, and J. Asher, *Phys. Rev. C* **39**, 2256 (1989).
- [19] D. P. Singh Unnati, P. P. Singh, A. Yadav, M. K. Sharma, B. P. Singh, K. S. Golda, R. Kumar, A. K. Sinha, and R. Prasad, *Phys. Rev. C* **80**, 014601 (2009).
- [20] S. Dutt, A. Agarwal, M. Kumar, V. R. Sharma, I. A. Rizvi, R. Kumar, and A. K. Chaubey, *EPJ Web Conf.* **66**, 03024 (2014).
- [21] S. Dutt, A. Agarwal, M. Kumar, K. Kumar, I. A. Rizvi, R. Kumar, and A. K. Chaubey, *EPJ Web Conf.* **86**, 00009 (2015).
- [22] S. A. Tali, H. Kumar, M. A. Ansari, A. Ali, D. Singh, R. Ali, P. K. Giri, S. B. Linda, R. Kumar, S. Parashari, S. Muralithar, and R. P. Singh, *Phys. Rev. C* **100**, 024622 (2019).
- [23] P. K. Giri, D. Singh, A. Mahato, S. B. Linda, H. Kumar, S. A. Tali, S. Parasari, A. Ali, M. A. Ansari, R. Dubey, R. Kumar, S. Muralithar, and R. P. Singh, *Phys. Rev. C* **100**, 024621 (2019).
- [24] A. Chauhan, M. Maiti, and S. Lahiri, *Phys. Rev. C* **99**, 064609 (2019).
- [25] E. R. Schachner, M. C. Gil, H. L. Atkins, P. Som, S. C. Srivastava, J. Badia, D. F. Sacker, R. G. Fairchild, and P. Richards, *J. Nucl. Med.* **22**, 352 (1981).
- [26] H. Morgenstern, W. Bohne, W. Galster, K. Grabisch, and A. Kyanowski, *Phys. Rev. Lett.* **52**, 1104 (1984).
- [27] P. P. Singh, B. P. Singh, M. K. Sharma Unnati, D. P. Singh, R. Prasad, R. Kumar, and K. S. Golda, *Phys. Rev. C* **77**, 014607 (2008).
- [28] M.. Shuaib, V. R. Sharma, A. Yadav, P. P. Singh, M. K. Sharma, D. P. Singh, R. Kumar, R. P. Singh, S. Muralithar, B. P. Singh, and R. Prasad, *Phys. Rev. C* **94**, 014613 (2016).
- [29] O. B. Tarasov and D. Bazin, *Nucl. Instrum. Methods Phys. Res., Sect. B* **266**, 4657 (2008); A. Gavron, *Phys. Rev. C* **21**, 230 (1980); <http://lise.nscl.msu.edu/pace4>.
- [30] The stopping and range of ions in matter (SRIM) code, <http://www.srim.org/SRIM/SRIMLEGL.htm>.
- [31] CANDLE, Data acquisition and analysis software, designed to support the accelerator-based experiments at the Inter University Accelerator Centre (IUAC), New Delhi, India.
- [32] E. Browne and R. B. Firestone, *Table of Radioactive Isotopes* (Wiley, New York, 1986).
- [33] W. Hauser and H. Feshbach, *Phys. Rev.* **87**, 366 (1952).
- [34] R. Bass, *Phys. Rev. Lett.* **39**, 265 (1977).
- [35] F. D. Becchetti and G. W. Greenlees, *Phys. Rev.* **182**, 1190 (1969).
- [36] A. Gilbert and A. G. W. Cameron, *Can. J. Phys.* **43**, 1446 (1965).
- [37] M. Cavinato, E. Fabrici, E. Gadioli, E. Gadioli Erba, P. Vergani, M. Crippa, G. Colombo, I. Redaelli, and M. Ripamonti, *Phys. Rev. C* **52**, 2577 (1995).
- [38] A. Sharma, B. B. Kumar, S. Mukherjee, S. Chakrabarty, B. S. Tomar, A. Goswami, and S. B. Manohar, *J. Phys. G: Nucl. Part. Phys.* **25**, 2289 (1999).
- [39] A. Agarwal *et al.*, Proc. DAE-BRNS Symp. Nucl. Phys. **64**, B69 (2019).
- [40] S. Ali, K. Kumar, M. Gull, T. Ahmad, I. A. Rizvi, A. Agarwal, A. K. Chaubey, and S. S. Ghugre, *Phys. Rev. C* **100**, 064607 (2019).
- [41] S. A. Tali *et al.*, *Nucl. Phys.* **A970**, 208 (2018).
- [42] V. R. Sharma, A. Yadav, P. P. Singh, D. P. Singh, S. Gupta, M. K. Sharma, I. Bala, R. Kumar, S. Murlithar, B. P. Singh, and R. Prasad, *Phys. Rev. C* **89**, 024608 (2014).
- [43] H. Kumar *et al.*, *Nucl. Phys.* **A960**, 53 (2017).